GLIA

Received: 10 March 2022 Revised: 3 June 2022 Accepted: 5 June 2022

DOI: 10.1002/glia.24230

RESEARCH ARTICLE

WILEY

Regional and age-related diversity of human mature oligodendrocytes

Moein Yaqubi[1] | Julia Xiao Xuan Luo[1] | Salma Baig[2] | Qiao-Ling Cui[1] | Kevin Petrecca[2] | Haritha Desu[3] | Catherine Larochelle[3] | Elia Afanasiev[1] | Jeffery A. Hall[2] | Roy Dudley[4] | Myriam Srour[5] | Lisbet Haglund[6] | Jean Ouellet[6,7] | Miltiadis Georgiopoulos[2,6] | Carlo Santaguida[7] | Joshua A. Sonnen[8] | Luke M. Healy[1] | Jo Anne Stratton[1] | Timothy E. Kennedy[1,2] | Jack P. Antel[1]

[1]Neuro-immunology Unit, Montreal Neurological Institute and Department of Neurology and Neurosurgery, McGill University, Montreal, Canada

[2]Department of Neurology and Neurosurgery, Montreal Neurological Institute, McGill University, Montreal, Canada

[3]Department of Neurosciences, Centre de Recherche du Centre Hospitalier de l'Université deMontréal, Montreal, QC, Canada

[4]Department of Pediatric Neurosurgery, Montreal Children's Hospital, Montreal, Canada

[5]Division of Pediatric Neurology, Montreal Children's Hospital, Montreal, Canada

[6]The Orthopedic Research Laboratory, Department of Surgery, McGill University, Montreal, Canada

[7]McGill Scoliosis and Spine Group, Department of Surgery, McGill University, Montreal, Canada

[8]Departments of Pathology, Neurology and Neurosurgery, McGill University, Montreal, QC, Canada

Correspondence
Jack P. Antel, Neuro-immunology Unit, Montreal Neurological Institute and Department of Neurology and Neurosurgery, McGill University, Montreal, Canada.
Email: jack.antel@mcgill.ca

Graphical Abstract

The contents of this page will be used as part of the graphical abstract of html only. It will not be published as part of main.

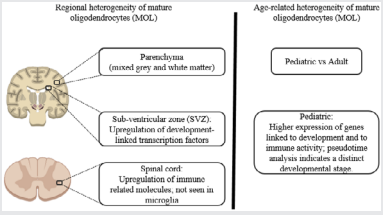

scRNA sequencing identified regionally distinct mature oligodendrocytes (OL) subpopulations in the adult human CNS, including relative expression of immune markers. Pediatric OLs retain higher expression of genes linked to development and to immune activity.

SPi	Journal Code	Article ID	Dispatch: 16-JUN-22	CE:
	GLIA	24230	No. of Pages: 12	ME:

Received: 10 March 2022 | Revised: 3 June 2022 | Accepted: 5 June 2022

GLIA

WILEY

DOI: 10.1002/glia.24230

RESEARCH ARTICLE

Regional and age-related diversity of human mature oligodendrocytes

Moein Yaqubi[1] | Julia Xiao Xuan Luo[1] | Salma Baig[2] | Qiao-Ling Cui[1] | Kevin Petrecca[2] | Haritha Desu[3] | Catherine Larochelle[3] | Elia Afanasiev[1] | Jeffery A. Hall[2] | Roy Dudley[4] | Myriam Srour[5] | Lisbet Haglund[6] | Jean Ouellet[6,7] | Miltiadis Georgiopoulos[2,6] | Carlo Santaguida[7] | Joshua A. Sonnen[8] | Luke M. Healy[1] | Jo Anne Stratton[1] | Timothy E. Kennedy[1,2] | Jack P. Antel[1]

[1]Neuro-immunology Unit, Montreal Neurological Institute and Department of Neurology and Neurosurgery, McGill University, Montreal, Canada

[2]Department of Neurology and Neurosurgery, Montreal Neurological Institute, McGill University, Montreal, Canada

[3]Department of Neurosciences, Centre de Recherche du Centre Hospitalier de l'Université deMontréal, Montreal, QC, Canada

[4]Department of Pediatric Neurosurgery, Montreal Children's Hospital, Montreal, Canada

[5]Division of Pediatric Neurology, Montreal Children's Hospital, Montreal, Canada

[6]The Orthopedic Research Laboratory, Department of Surgery, McGill University, Montreal, Canada

[7]McGill Scoliosis and Spine Group, Department of Surgery, McGill University, Montreal, Canada

[8]Departments of Pathology, Neurology and Neurosurgery, McGill University, Montreal, QC, Canada

Correspondence
Jack P. Antel, Neuro-immunology Unit, Montreal Neurological Institute and Department of Neurology and Neurosurgery, McGill University, Montreal, Canada.
Email: jack.antel@mcgill.ca

Abstract

Morphological and emerging molecular studies have provided evidence for heterogeneity within the oligodendrocyte population. To address the regional and age-related heterogeneity of human mature oligodendrocytes (MOLs) we applied single-cell RNA sequencing to cells isolated from cortical/subcortical, subventricular zone brain tissue samples, and thoracolumbar spinal cord samples. Unsupervised clustering of cells identified transcriptionally distinct MOL subpopulations across regions. Spinal cord MOLs, but not microglia, exhibited cell-type-specific upregulation of immune-related markers compared to the other adult regions. SVZ MOLs showed an upregulation of select number of development-linked transcription factors compared to other regions; however, pseudotime trajectory analyses did not identify a global developmental difference. Age-related analysis of cortical/subcortical samples indicated that pediatric MOLs, especially from under age 5, retain higher expression of genes linked to development and to immune activity with pseudotime analysis favoring a distinct developmental stage. Our regional and age-related studies indicate heterogeneity of MOL populations in the human CNS that may reflect developmental and environmental influences.

KEYWORDS
immune oligodendrocyte, pseudotime, regional heterogeneity, single-cell RNAsequencing, temporal heterogeneity

1 | INTRODUCTION

Classic functions for oligodendrocyte (OLs) include myelinating axons to permit efficient saltatory nerve conduction and providing trophic support to neurons. Experimental demyelination models indicate that mature OLs (MOLs) can also participate in the process of remyelination, a process that is usually attributed to the recruitment and differentiation of progenitor cells (Duncan et al., 2018; Franklin & Ffrench-Constant, 2008).

Although the human brain parenchyma has abundant numbers of progenitor cells (*PDGFRA*+ and *NG2*+), carbon 14-based studies of adult human brain parenchyma (Yeung et al., 2019) indicate that once

OL lineage cells have matured, they are long-lived with little turnover, although their myelin membranes are highly plastic (Yeung et al., 2019). A central question is whether the various OL functions can be linked to the heterogeneity of cells within the overall OL population. OL heterogeneity, based on morphologic features, has been suggested since their initial description (Pérez-Cerdá et al., 2015), including that of developmental heterogeneity between the spinal cord and those that populate the telencephalon (Foerster et al., 2019). Internodal length is greater in spinal cord. More recent findings have described the roles for OLs regulating central nervous system (CNS) inflammation through the expression of surface molecules that support cellular immune responses and by producing cytokines (Falcão et al., 2018; Jäkel et al., 2019; Kirby et al., 2019).

Single-cell (sc) and single nuclear (sn) RNA sequencing (RNAseq) technologies are increasingly being used to define the transcriptional heterogeneity of OL lineage cells (Chen et al., 2017; Habib et al., 2017; Marques et al., 2016, 2018; Zeisel et al., 2015). Such studies define the molecular signature of MOLs based on the expression of cell type-specific canonical marker genes. Previous studies have revealed OL lineage cells that express distinct transcriptional profiles in juvenile and adult mice in an age- and region-dependent manners (Marques et al., 2016). However, differences have also been identified in the transcriptomic and proteomic content of myelin between humans and mice (Ishii et al., 2009). Studies of the transcriptional heterogeneity of human OL lineage cells at the single-cell level (Darmanis et al., 2015; Jäkel et al., 2019; Lake et al., 2018; Perlman et al., 2020; Spaethling et al., 2017) have utilized cerebral tissue samples. Adult human post-mortem single nuclei (sn)RNA sequencing studies have included comparison of different cerebral regions (Habib et al., 2017; Lake et al., 2018). Studies using surgical samples also have used only cerebral tissue and involved limited cell numbers (Spaethling et al., 2017).

The initial aim of our study was to identify regional heterogeneity of MOLs across human CNS by comparing transcriptional landscape of cells derived from cortical/subcortical (referred to as parenchyma), subventricular (SVZ), and spinal cord (SC) regions at single whole-cell level using scRNA sequencing technique. We considered whether such heterogeneity may either be determined by lineage differences or reflect local environmental signals. The parenchyma samples were obtained from surgical resections; the thoracolumbar SC samples from rapid post-mortems of organ donors. Both contained white and gray matter. MOLs derived from SVZ surgical samples (Figure S1a & b) were derived from locations adjacent to a specialized niche enriched with neural progenitor cells.

We further aimed to examine age-related transcriptional heterogeneity of human MOLs by comparing adult and pediatric surgically derived parenchyma samples. Our previous in vitro studies indicate that MOLs derived from younger donors are more susceptible to metabolic stress-induced injury compared to adult donors (Fernandes et al., 2021) suggesting age-related heterogeneity of MOL. Our additional studies have also indicated that human MOLs from pediatric donors ensheath nanofibers more efficiently than adult-derived cells although significantly less than A2B5 + cells (also known as pre-OLs) derived from the same tissue samples (Luo et al., 2022).

To facilitate the use of our scRNA-seq datasets, we have also developed a straightforward online tool for evaluating gene expression at single-cell resolution (https://stratton-lab.github.io/dataviz).

2 | RESULTS

2.1 | Regional heterogeneity of adult-derived mature oligodendrocyte populations

To address regional MOL heterogeneity, we utilized single whole-cell RNA-sequencing datasets derived from the total cell population isolated from the adult cortical/subcortical parenchyma, thoracolumbar spinal cord (SC), and the MOL population selected from the subventricular (SVZ) region dataset ($n = 3$ per region) (Table S1). Each individual dataset was subjected to a pre-processing step and after quality control, we obtained 21,114 cells. All datasets were then integrated into a single object for the downstream analysis. We identified seven cell types in our analysis including MOL, microglia, border-associated macrophages (BAM), T cells, OPCs, astrocytes, and endothelial cells (EC) according to the enriched expression of marker genes for each cell type (Figure 1a & b). MOLs were selected for further analysis based on the expression of the canonical MOL marker genes; myelin-associated glycoprotein (*MAG*) and proteolipid protein 1 (*PLP1*) with the exclusion of OPC marker genes *PDGFRA* and *PTPRZ1* (Figure 1c). The isolated MOLs were randomly downsampled to ensure that the observed result was not skewed by differing cell numbers. We provide a supplementary table (Table S2) to show that the expected myelin proteins are specifically upregulated in our MOL population when compared with OL progenitor cells (OPCs) and microglia, the latter being the other main glial population present in our isolated cell populations.

The downsampled MOLs were then re-clustered to discern more detailed differences between each anatomical location according to their transcriptome. A small population of the isolated cells expressing microglia markers such as AIF1 was considered contaminants and excluded from downstream analysis, resulting in 1264 cells per region (not shown). Re-clustering of these cells resulted in the identification of six distinct subpopulations of MOLs with differential distribution patterns between anatomical regions and within each subpopulation (Figure 1d & e). Hierarchal clustering of cells according to the expression of the top five upregulated genes in each subpopulation indicates that while each subpopulation has a specific gene expression signature, overall there exists a continuum of gene expression between subpopulations (Figure 1f; Table S3). Gene ontology analysis of the upregulated genes per subpopulation indicated specific function-associated processes for each MOL subpopulation (Figure 1g). All anatomical regions contributed to subpopulations 1, 2, and 6 in which pathway analysis featured enrichment of myelination, axon engagement, and elaboration of cellular processes-related terms; all well-characterized properties of MOLs (Figure 1g). Subpopulations 3 and

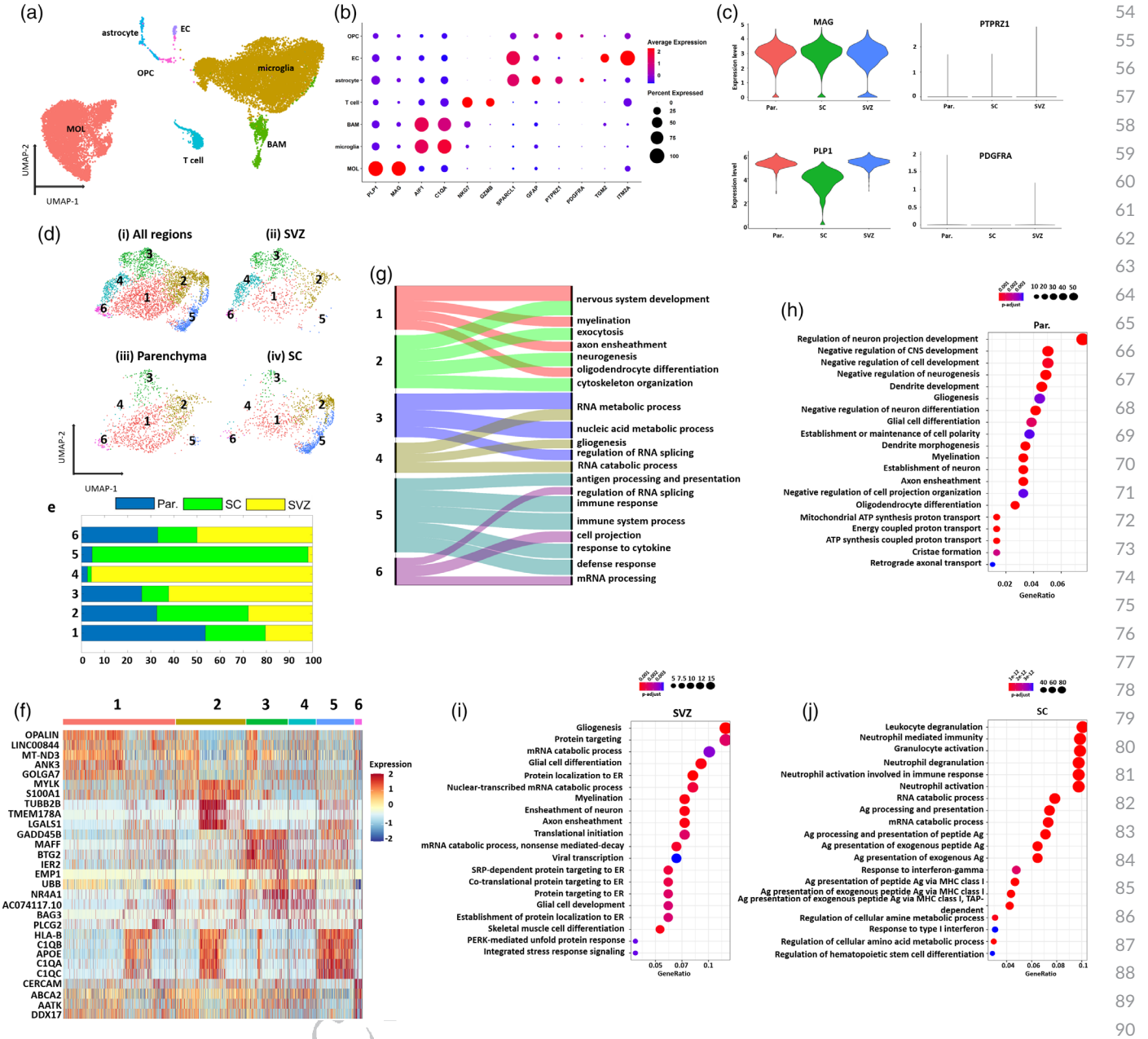

FIGURE 1 Distinct subpopulations of human MOLs across different regions of adult CNS. (a) UMAP plot of 22,096 captured cells across three anatomical regions of nine adult donors depicting seven major cell types. (b) Dotplot presents canonical markers of each identified cell types. The circle size denotes the percentage of cells that express each individual gene. Average gene expression is represented using color-coded z-scores. (c) Violin plot depicts normalized expression of mature oligodendrocyte marker genes (*PLP1* and *MAG*) and oligodendrocyte progenitor cells (*PDGFRA* and *PTPRZ1*). (d) UMAP plot represents six subpopulations of mature oligodendrocytes (MOLs) across all regions (i) and each anatomical location individually (ii–iv). (1296 cells per anatomical location) (e) Stacked bar plot of the abundance of cells from each anatomical location per subpopulation. Each location is represented by a different color. (f) Heatmap of the five most differentially upregulated genes per subpopulation (adjusted $p < .05$ based on the negative binomial distribution). The expression of genes is represented using color-coded z-scores. Red and blue colors denote high and low expression of genes, respectively. (g) Alluvial plot showing biological pathway analysis of the most upregulated genes per subpopulation. The most affected biological processes of each subpopulation on the right side of the plot are connected to subpopulations on the left side by a ribbon. The width of each ribbon indicates the number of genes present in each term. (h–i) Biological pathway analysis of upregulated genes in parenchyma, SVZ, and SC samples, respectively. The most affected biological processes are represented. The size of the dots represents the number of genes per term and the color of the dots represents the adjusted *p*-values of the terms.

4 were enriched with cells from the SVZ region, for which pathway analysis identified associations with gliogenesis and RNA processing terms (Figure 1g). In subpopulation 5, we detected an enrichment of immune-related terms among the most affected biological processes (Figure 1g) with SC-derived cells being the main contributor to this subpopulation (Figure 1e).

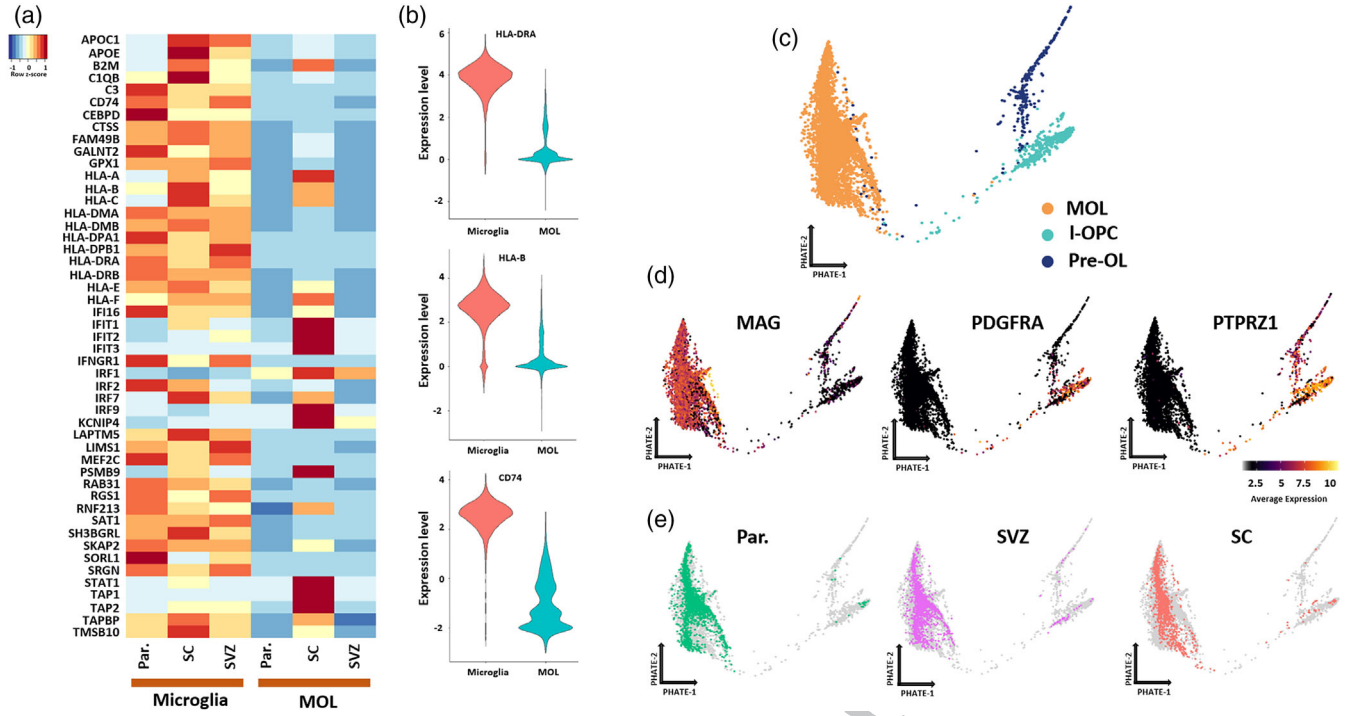

FIGURE 2 Distinct gene expression signature of human MOLs across various regions of CNS. (a) Heatmap representing the expression of immune genes derived from reports of Jäkel et al., 2019, Kirby et al., 2019, and Falcão et al., 2018 on MOLs and microglia for each region in our dataset. The expression of genes is represented using color-coded z-scores. Red and blue colors denote high and low expression of genes, respectively. (b) Violin plots shows normalized gene expression of immune markers enriched in MOL and microglia across all regions. (c) PHATE visualization for primary post-natal OL lineage cells including late OL progenitors (lOPC), pre-oligodendrocytes (pre-OLs), and MOLs. (d) PHATE visualization represents the normalized expression of OL lineage cell marker genes. (e) PHATE visualization of OL lineage cells by region, including parenchymal, SVZ, and SC regions.

We then applied gene ontology (GO) analysis of the most upregulated genes in the total MOL population of each region. In line with our observations for MOL subpopulations analysis, GO terms for parenchymal cells were largely associated with canonical biological MOL processes such as axon ensheathment and myelination, regulation of neuron projection development, and maintenance of cell polarity (Figure 1h). For SVZ cells, in addition to identification of myelin-related terms, we observed significant enrichment of gliogenesis and RNA metabolic activity (Figure 1i). For SC cells, immune-related terms, including antigen presentation and response to interferon, were the most dominant affected biological processes (Figure 1j).

To examine the expression of immune-related genes of SC MOLs in more detail, we compiled markers of immune OL (iOL) from previous studies (Falcão et al., 2018; Jäkel et al., 2019; Kirby et al., 2019) and then plotted the expression of the compiled iOL markers against our datasets. This revealed that SC-derived MOLs showed notably higher expression of these iOL marker genes compared to parenchyma and SVZ regions (Figure 2a). These included genes involved in antigen presentation including major histocompatibility class I and II genes such as *HLA-DRA*, *HLA-B*, and *HLA-C* (Figure 2a; Table S4). This heightened immune signature was not observed when comparing SC microglia to parenchyma and SVZ microglia suggesting that enriched iOLs signature in SC is a unique feature for this cell type and not a general heightened immune signature across numerous cell types within the spinal cord (Figure 2a). As expected, the expression of immune genes was significantly less in MOLs as compared to microglia consistent with microglia being the major immune cell type in all regions (Figure 2b).

To address whether the regional findings reflect distinct developmental lineages, we performed pseudotime analysis by integrating the current dataset to our previous combined pediatric/adult brain parenchyma single-cell RNA sequencing datasets which contain OL progenitor cells including late (l)-OPCs, pre-oligodendrocytes (pre-OLs), and MOLs (Fernandes et al., 2021; Perlman et al., 2020) (Figure 2c). The expression of cell-type marker genes was used to annotate cells on the pseudotime trajectory plot (Figure 2d). This analysis documented the development pathway of OL lineage cells; a path which starts with l-OPCs, followed by pre-OLs and finally MOLs (Figure 2c). Moreover, in the MOL population, we observed a clear overlap from different anatomical locations suggesting mature adult cells from the different regions have similar lineage trajectories (Figure 2e). Based on the pseudotime analysis, we suggest that the detected transcriptional differences between MOLs in the different regions do not reflect a distinct stage in the developmental lineages and may reflect responses to their surrounding microenvironments. There was also no region-linked expression of cell cycle-related genes, confirming the maturity of the cells (Figure S1c).

In addition, we compared the molecular signature of our adult parenchymal MOLs with existing reports on the heterogeneity of human mature OLs[−1], focusing on common differentially upregulated genes within defined subpopulations. We compared the expression signature of the five MOLs and one immune OL subpopulation identified using our adult parenchymal samples (Figure S1d) with seven MOL subpopulations identified (including immune OL) in the Jäkel et al study (Jäkel et al., 2019). The percent of overlap between upregulated genes in two studies varied among subpopulations (Figure S1e), both identify an immune OL subpopulation. The highest overlap was between upregulated genes in our MOL1 population and with subpopulations 1 and 5 of the Jäkel et al study (Figure S1e).

2.2 | Age-related heterogeneity of mature oligodendrocytes

We next sought to investigate age-related heterogeneity of MOLs. To this end, single-cell RNA sequencing was performed on cells derived from four adult parenchymal samples including three used in the regional studies and seven pediatric parenchyma samples. Following quality control, all sequenced cells (46,066 cells) were integrated into one dataset for downstream analysis in which we identified microglia, oligodendrocyte lineage cells including MOLs and OL progenitors, astrocytes, and lymphocytes (Figure 3a). Consistent with the regional analysis, MOLs were selected for the downstream analysis using the expression of *PLP1* and *MAG* with the exclusion of cells expressing *PDGFRA* or *PTPRZ1* (Figure 3b).

Unsupervised clustering of the selected cells resulted in the identification of four MOL subpopulations (MOL[i-iv]) (Figure 3c; Table S5) which, as shown in "d," expressed *MAG* and did not express the progenitor markers *PDGFRA* and *PTPRZ1* (Figure 3d). A small population corresponding to subpopulation four (MOL[iv]) also expressed the immune marker *CD74* (Figure 3d). Comparisons of the four identified MOL subpopulations indicated that MOL (i-iii) presented a continuum of transcriptome content while MOL (iv) had the most distinct signature (Figure 3e; Table S5). MOL (i) expressed a series of early stress response genes such as early growth response 1 (*EGR1*) and heat shock protein family A (*Hsp70*) member 1A (*HSPA1A*) (Figure 3e); this subpopulation was observed in both pediatric and adult samples (data not shown). MOL (ii) exhibited notable upregulation of oligodendrocytic myelin paranodal and inner loop protein (*OPALIN*) (also known as *TMEM10*) which is associated with axon myelination in vivo (de Faria et al., 2019) and tubulin polymerization promoting protein (*TPPP*) which regulates microtubule nucleation and promotes OL internode elongation (Fu et al., 2019). The transcriptomic signature of MOL (iii) differentially upregulated expression of myosin light chain kinase (*MYLK*) which has been described to mark MOLs as a "late differentiation gene" (Yu et al., 2013) and finally MOL (iv) was enriched in immune-related genes as defined by Jäkel et al., 2019 (Jäkel et al., 2019).

To assess the functional properties of these MOL subpopulations, we performed pathway analysis for the subpopulation-specific gene sets. Consistent with the transcriptomic observation MOL (i) was enriched with terms related to cellular response to stress. MOL (ii) showed terms enriched with axon ensheathment and myelination, MOL (iii) was mainly enriched for lipid metabolism such as cholesterol biosynthetic process, and MOL (iv) was enriched for immune-related pathways (Figure 3f).

To compare the relative levels of MOL gene expression across the age groups, we examined the dataset independent of identified subpopulations by directly comparing pediatric with adult samples (Figure 4a & b; Table S6). The pediatric samples showed increased expression of iOL markers, including major histocompatibility complex, class I, A-C, (*HLA-A*, *HLA-B*, *HLA-C*) (Falcão et al., 2018; Jäkel et al., 2019) and OL maturation-related genes including SRY-box transcription factor 2 (*SOX2*), NK6 homeobox 2 (*NKX6-2*) and oligodendrocyte transcription factor 2 (*OLIG2*) (Figure 4a & b; Table S6) (Cai et al., 2010; Küspert et al., 2011; Zhao et al., 2015). Pathway analysis indicated that adult MOLs were enriched with terms related to metabolism (Figure 4c) while pediatric samples were enriched with pathways related to development and immune reactivity (Figure 4d). Since the pediatric samples covered a wide age range from 2 years up to 14-year-old individuals, we divided the pediatric samples into less than 5 years and greater than 5-year-old groups, based on the age distribution of the available samples. Although we did not find a differential distribution of MOL subpopulations across these age groups within each subpopulation (Figure 4e), the observed upregulation of development and immune-related terms in the pediatric group mainly resulted from genes upregulated in the younger cohort (Figure 4f) compared to the older samples (Figure 4g). We observed that MOLs derived from pediatric samples less than 5 years old have comparable levels of expression of iOL genes with lOPC (Figure 4h).

As for our regional analysis, we performed pseudotime analysis to assess the developmental trajectory of pediatric MOLs (Figure 4i). l-OPCs, and pre-OLs followed a tight trajectory whereas the path notably broadens upon reaching the MOLs (Figure 4i). MOLs of pediatric samples <5 years old clustered more closely toward the pre-OLs compared to MOLs of those from more than 5 years old and adult samples, suggesting potential developmental differences between MOLs at different ages of human development (Figure 4j).

Our parenchymal and spinal cord tissue samples contained elements of both white and gray matter (WM and GM). To examine differential immune-related gene expression of WM and GM we separated white and gray tissue fragments based on visual inspection from selected parenchymal cases and subjected these to the standard isolation procedure. FACS analyses indicated that a relatively greater number of OLs (O4 + cells) from white matter, while a greater number of microglia (CD11b+) cells were derived from GM (Figure S2a–c). OLs (O4 + cells) from both regions had a negligible expression of MHC class 1 and no class II; MHC class II was detected on microglia with some increase in WM samples (Figure S2d–g). qPCR analysis showed a prominent HLA-DR signal in both GM and WM. MHC class 1 expression was detectible but low and comparable between GW and WM samples (Figure S2h–i).

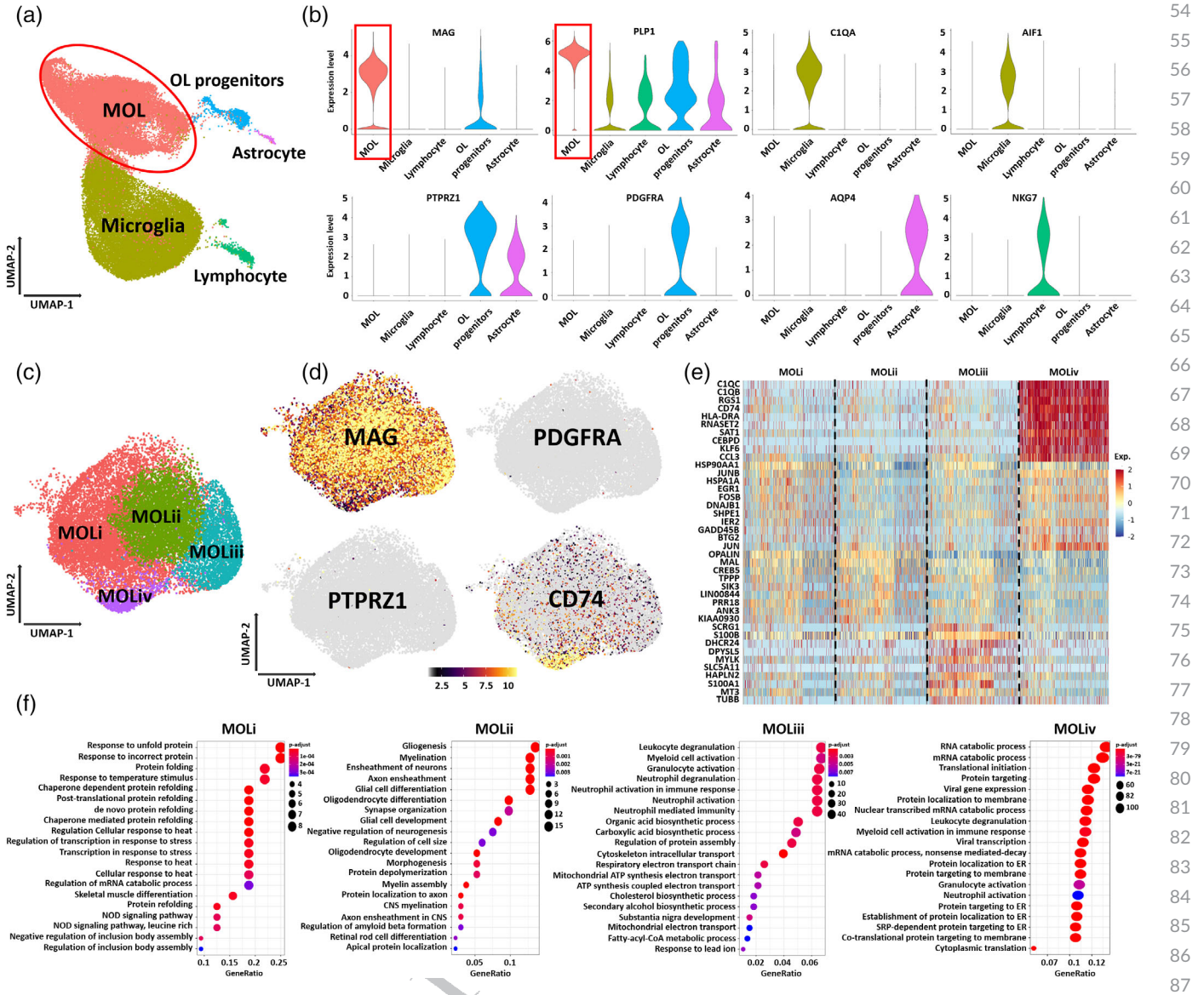

FIGURE 3 scRNA-seq identifies transcriptionally distinct subpopulations of human MOLs across different ages of human development. (a) UMAP plot of 46,066 sequenced cells from 11 pediatric and adult donors depicts five major cell types. The red circle denotes MOLs which were used for the downstream analysis. (b) Violin plot depicting normalized expression of cell type-specific markers. The red rectangles show *MAG*+ and *PLP1*+ cells which were selected for the downstream analysis. (c) UMAP plot represents four subpopulations of MOLs across all ages. (d) UMAP plot represents normalized expression of MOL (*MAG*), OL progenitor cells (*PTPRZ1* and *PDGFRA*), and immune OLs (*CD74*). (e) Heatmap of the 10 most differentially upregulated genes per subpopulation (adjusted $p < .05$ based on the negative binomial distribution). The expression of genes is represented using color-coded *z*-scores. Red and blue colors denote high and low expression of genes, respectively. (f) Biological process analysis of the upregulated genes per subpopulation. The size of the dots represents the number of genes per GO term and the color of the dots represents the adjusted *p*-values of the terms.

3 | DISCUSSION

Our access to a combination of surgically and rapid post mortem obtained adult tissue samples provided the opportunity to identify regional and age-related heterogeneity of mature oligodendrocytes (MOLs) in human central nervous system, using whole single-cell RNA sequencing technique. For the parenchymal adult and pediatric tissue samples, the collected brain tissue was obtained from normal appearing superficial surgical tissue that was removed to access the area of underlying non-malignant underlying pathology. These samples were enriched in white matter tissue but also contained gray matter. Neuropathologic analysis of CUSA tissue samples confirmed that the fragments were predominantly comprised of histologically normal tissue although there were some fragments reflecting the underlying pathology. Our analysis did not detect specific gene signatures of OLs enriched in gray matter, such as peri-neuronal OLs that feature a distinct transcriptional profile (Bernstein et al., 2019; Szuchet et al., 2011). The SVZ adjacent samples were obtained from surgical cases of glioma

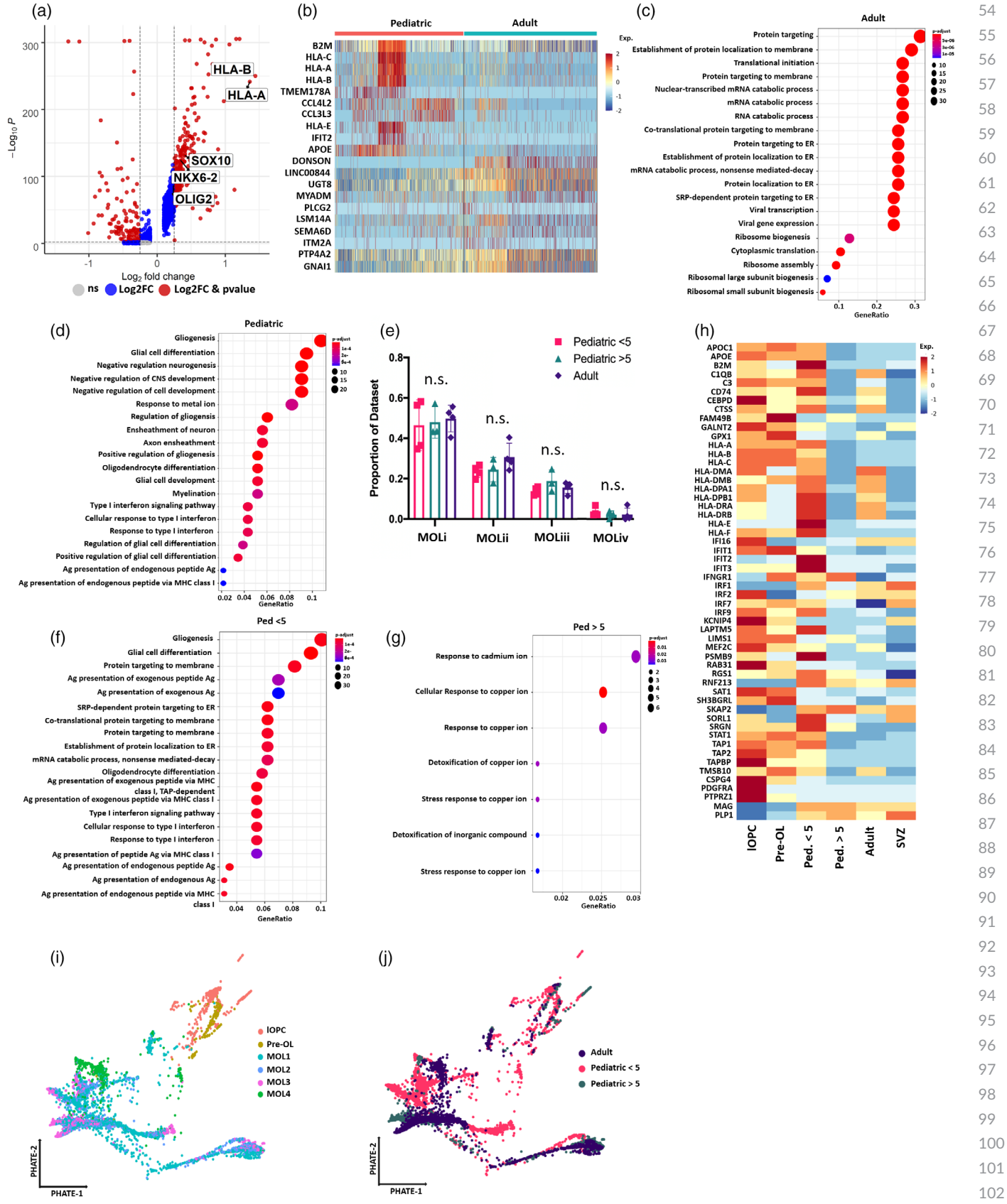

FIGURE 4 Legend on next page.

but were distinct from visible tumor sites. The MOL population was selected out from a total cell population that was enriched for progenitor cells contained within this niche. Our spinal cord (SC) samples are from individuals who did not have any background disease.

The molecular comparisons of MOLs from three distinct regions of the adult CNS indicated that SC MOLs significantly upregulate immune-related markers as listed in (Falcão et al., 2018; Jäkel et al., 2019; Kirby et al., 2019) compared to MOLs derived from the brain. Jäkel and colleagues found iOLs to be enriched in post mortem white matter samples from cases of multiple sclerosis compared to controls (Jäkel et al., 2019). As noted, we did not observe such upregulation of immune-related markers in microglia of SC versus such cells from other regions The observed difference between MOLs and microglia may be due to the specific interactions of OL lineage cells and neuronal subtypes in local microenvironments across different CNS regions as suggested by (Zonouzi et al., 2019). Seeker et al detected the expression of an immune-gene expressing OL cluster in the human cervical spinal cord (Seeker et al., 2022).

Our study shows that MOLs of the SVZ have increased expression of selective progenitor features even though they do exhibit the classic expression profile of OL progenitor makers (*PDGFRA* and *PTPRZ1*). Gene ontology analysis of the most upregulated genes of SVZ MOLs showed enrichment of RNA metabolic process and gliogenesis. In parallel, among the list of significantly upregulated genes in this region, we found enrichment of regulatory factors which have been shown to be critical for the maintaining progenitor state of OL lineage cells, including oligodendrocyte transcription factor 1 (*OLIG1*), SRY-box transcription factor 10 (*SOX10*) and POU Class 3 Homeobox 1 (*POU3F1*) (Aprato et al., 2020; Arnett et al., 2004; Fulton et al., 2011). However, our pseudotime analysis indicated these observations do not reflect a precise development stage in this region. We postulate that the microenvironment of the SVZ, as the largest neurogenic zone of the brain (Martínez-Cerdeño & Noctor, 2018), may provide a cellular niche which favors persistent retention of selective developmental characteristics. The absence of cell cycle-related genes supports the notion that these cells are not classic progenitor cells and therefore form a distinct population of mature cells around the SVZ region.

Our pseudodtime analysis of the current dataset with our previous combined pediatric/adult brain dataset identified a distinct population of pre-OLs. "Pre-OLs" defined by being recognized by A2B5 ganglioside-directed antibody are shown to comprise 3–5% of the OL lineage cells present in the adult human brain; A2B5 antibody used to isolate such cells. Since these A2B5+ cells are defined by a ganglioside and not a specific protein/gene, we cannot precisely match them to the molecularly defined late- and pre-OLs. Transplant-based studies using such cells by Windrem et al (Windrem et al., 2004) and our studies applying these cells to nanofiber-containing cultures (Luo et al., 2022) indicate these cells can differentiate, ensheath, and myelinate.

Our previous studies of parenchyma-derived MOLs indicated age-linked differences in functional properties related to susceptibility to injury and process outgrowth (Fernandes et al., 2021). Comparing the gene expression profile of MOLs from pediatric and adult-derived cells indicated that the pediatric cells (specifically those from individuals younger than 5 years old) have more progenitor features, due to higher expression of critically important genes such as *NKX6-2*, *OLIG2*, and *SOX10*, all of which have been shown to be important for the progenitor state of the cells (Aprato et al., 2020; Cai et al., 2010; Küspert et al., 2011). The pediatric samples showed increased expression of immune OL markers. The expression of these markers in OL lineage cells is lower than in myeloid cells derived from the same samples. In a previous study, we applied bulk RNA sequencing to enriched populations of pre-OLs (A2B5 + cells) and mature OLs (A2B5-cells) derived from adult and pediatric parenchymal samples using in vitro immuno-magnetic-based separation (Luo et al., 2022). We reported that OL-progenitor markers were upregulated in the pre-OLs compared to the mature OLs and in the pediatric pre-OLs as compared to the adult. Our current detailed re-analysis of the supplementary dataset from that study (Supplementary Datasets in Luo et al., 2022 indicated persistent enrichment of immune-related and development-related biological pathways (i.e., cell proliferation) in the pediatric samples as compared to the adult, correlating with our findings in the current single-cell dataset. Our pseudotime analysis of ex vivo cells was able to define an overall less mature developmental stage in contrast to the adult SVZ MOLs Our numbers are too limited to determine a

FIGURE 4 Gene expression differences between pediatric and adult MOLs. (a) Volcano plot showing differentially expressed genes between pediatric and adult donors. The genes that are verified by fold change and p-value are represented by red and blue colors, respectively. The gray dots denote non-significant genes. The names of OL development-associated transcription factors and major histocompatibility genes which are upregulated in pediatric samples are shown on the volcano plot. (b) Heatmap plot showing the 10 most differentially upregulated genes in pediatric and adult samples (adjusted $p < .05$ based on the negative binomial distribution). The expression of genes is represented using color-coded z-scores. (c–d) Biological process analysis of the upregulated genes in adult samples (c), pooled pediatric samples (d). The size of the dots represents the number of genes per pathway and the color of the dots represents the adjusted *p*-values of the terms. (e) Proportion of MOLs from different ages within each identified subpopulation. n.s. stands for not significant. (f–g) Biological process analysis of the upregulated genes in pediatric samples less than age 5 (f) and over 5 (g). The size of the dots represents the number of genes per GO term and the color of the dots represents the adjusted p-values of the terms. (h) Heatmap representing the expression of immune oligodendrocyte genes, as derived from Jäkel et al., 2019, Kirby et al., 2019, and Falcão et al., 2018 studies on the following: lOPC and pre-OLs from our initial parenchymal pediatric samples Fernandes et al., 2021 study (Fernandes et al., 2021); MOLs from our overall pediatric parenchymal samples <5 and >5; MOLs from adult parenchymal and SVZ samples. The expression of genes is represented using color-coded z-score. Red and blue colors denote high and low expression of genes, respectively. (i) PHATE plot showing the trajectory analysis of OL lineage cells in post-natal brain parenchymal samples of pediatric and adult donors. Each cell type including the MOL subpopulation is represented using different colors. (j) PHATE plot showing the trajectory analysis of OL lineage cells by age.

gradient of age-related changes although our analyses of ensheathment capacity of human OPC lineage cells suggest that the superiority of pediatric age cells extends into adolescence age.

Our current single whole-cell RNA-seq analysis of the transcriptional heterogeneity of human MOLs provides direct evidence regarding regional, as well as age-related, heterogeneity of MOLs. We acknowledge the limitation that samples from different regions were collected under different conditions and that the different regions could not be sampled from the same donor given limited access to whole brain and spinal cords. Further studies will be needed to define the range of functional properties linked to the observed regional and age-related molecular heterogeneity and how these contribute to the extent of tissue injury and repair observed in cases of multiple sclerosis.

4 | METHODS

4.1 | Isolation and processing of the brain parenchyma, subventricular zone, and spinal cord tissues

Human brain parenchyma tissues were obtained from patients who underwent surgical procedures for indications listed in Table S1. Using a cavitron ultrasonic aspirator (CUSA), the samples were collected from normal-appearing superficial tissue that had to be removed to allow the neurosurgeon to reach the area of underlying pathology. Tissues from the normal-appearing CUSA bag material and from pathologic site resected material were subjected to neuropathologic examination. The use of adult brain tissues was approved by the Montreal Neurological Institute and Hospital (MNI/H) Neurosciences Research Ethics Board; the use of pediatric samples was approved by the Montreal Children's Hospital Research Ethics Board. The tissues were digested using mechanical and enzymatic (trypsin and DNase) dissociation followed by a Percoll gradient to remove the myelin layer (Leong et al., 2014). The dissociated cells were washed three times in PBS, and resuspended at a concentration of 10^6 cells per ml. Next, 100,000–200,000 cells were submitted for sequencing at Génome Québec.

Human thoracolumbar spinal cord tissue was harvested from organ donors through a collaboration with Transplant Quebec. All procedures were approved by and performed in accordance with the ethical review board at McGill University (IRB#s A04-M53-08B). Familial consent was obtained for each subject. The rapid autopsy spinal cord samples were processed within 2 hours of removal from the spinal column and tissue was kept on ice throughout. The samples were provided from the thoracolumbar region of the cord (T11-L1) of three adults, two females and one male; none were known to have prior neurologic disease. The cause of death is listed in Table S1. For tissue processing, the meninges were carefully removed, and the tissue was crosscut into small pieces of 1–2 mm^3. The subsequent tissue processing steps were similar to brain parenchyma samples.

Human ventral subventricular zone (SVZ) specimens were obtained from patients who underwent surgery for glioma resection. These samples were collected from tissue that had to be removed to access the area of underlying pathology; this tissue was MRI negative for tumor. As with the parenchymal specimens, the tissues were mechanically dissociated, then enzymatically digested (collagenase solution containing DNAase [Cal Biochem EMD Chemicals] and $MgCl_2$ for 1 h at 37°C), and centrifuged on a Percoll density gradient. Samples were then washed in PBS and submitted for sequencing. The mature OL fraction from the human SVZ region analyzed in this study was extracted from a larger dataset ($n = 3$) provided by Dr. Kevin Petrecca (KP) and that can be made available by KP upon request.

4.2 | Single-cell library preparation and sequencing

10x chromium technology was used to make the library of the cells. Briefly, single-cell RNA libraries were generated using the GemCode Single-Cell Instrument (10x Genomics, Pleasanton, CA, USA) and Single Cell 3' Library & Gel Bead Kit v2 and Chip Kit (P/N 120236 P/N 120237 10x Genomics). The Single Cell 3' Reagent Kits v2 user guide was followed for this step. The sequencing ready library was purified with SPRIselect, quality controlled for sized distribution and yield (LabChip GX Perkin Elmer), and quantified using qPCR (KAPA Biosystems Library Quantification Kit for Illumina platforms P/N KK4824). Finally, the sequencing was done using Illumina HiSeq4000 PE75 instrument (Illumina) at the McGill University and Génome Québec Innovation Centre.

4.3 | Single-cell RNAseq data analysis

All data demultiplexing and genome mapping were done using the Cell Ranger analysis pipeline (https://github.com/10XGenomics/cellranger). Reads were aligned to reference genome GRCh38. Individual datasets were subjected to standard Seurat pipeline (v 3.1) for quality control, gene expression normalization, batch-effect correction, clustering, and differential expression analysis (Stuart et al., 2019). Briefly, any cell with a genome comprised of 5 to 12 percent of mitochondrial genes was considered a dead cell and was removed from analysis. Similarly, any cell that contained <200 or more than 2500 unique feature counts was considered a low-quality cell and was removed from the downstream analysis. The gene expression levels of the cells were natural log normalized and scaled. The downstream analysis was restricted to 2000 highly variable genes for each dataset. At this point, individual datasets were integrated using the Seurat "FindIntegrationAnchors" and "IntegrateData" functions, which perform canonical correlation analysis (CCA) to remove any possible batch effect between datasets. Highly variable genes of the integrated object were identified and principle component analysis (PCA) was performed on them to reduce the dimensionality of the data. The first 20 principle components were selected for the purpose of clustering. A shared-nearest neighbor graph was constructed based on the PCA analysis and the Louvain clustering algorithm was used several times to identify clusters at multiple different resolutions (0.25 to 1). The clustree R package was used to construct a clustering tree and check the accuracy of the clustering(Zappia & Oshlack, 2018).

Finally, the uniform manifold approximation and projection (UMAP) algorithm was used to visualize the clusters in two-dimensional space. The expression levels of cell-type marker genes were used to determine the identity of each cluster. Differentially expressed genes between clusters and anatomical regions were identified using the "FindMarkers" function in Seurat based on Wilcox test scores for genes that were detected in at least 25% of cells in the populations compared. Heatmap plots of the top marker genes were generated using the DoHeatmap function. Clusterprofiler (v3.18) was used to do pathway analyses in the form over-representation analysis (ORA) using the "enrichGO" function and produce dot plots (Wu et al., 2021; Yu et al., 2012). Inputs were genes ranked by log2 fold change (logFC) and ORA was done for gene ontology biological processes (GO:BP). Gene ontology analysis for the regional heterogeneity part was performed using gProfiler web-tool and alluvial plot was made using MATLAB function. The volcano plot was generated using EnhancedVolcano (v1.8) package (Blighe & Rana, 2022).

4.4 | Pseudotime trajectory inference analysis of regional heterogeneity of mature oligodendrocytes

Pseudotime trajectory inference analysis was done using the PhateR (v1.0) package to order cells in "pseudotime" and visually highlight transitions between cells using dimensional reduction methods that minimize gene expression difference between sequential cell pairs. PhateR uses the "potential of heat diffusion for affinity-based embedding" (PHATE) method created by Moon et al., 2019 (Moon et al., 2019). Briefly, PHATE encodes local data via local similarities, encodes global relationships using potential distances based on diffusion probabilities, and embeds potential distance information into low dimensions via metric multi-dimensional scaling. The phate algorithm was run on the integrated counts derived from the Seurat object with the gamma parameter set to gamma = 0 and the remaining parameters set to default (knn = 5, decay = 40, optimal t was automatically selected to be t = 8). PhateR was chosen for the trajectory inference analysis as it does not rely on prior assumptions of data structure.

4.5 | Immunohistochemistry

Tissue samples from the SVZ region were subjected to IHC using the technique described in Couturier et al., 2020 (Couturier et al., 2020). MOLs were identified using MBP antibody anti-rabbit MBP ab216668. Briefly, slides with brain sections were baked overnight at 60°C then de-paraffinized and rehydrated using a graded series of xylene and ethanol, respectively. For heat-mediated antigen retrieval, slides were incubated in citrate buffer at 125°C for 20 min in a decloaking chamber (Biocare Medical), followed by a cool-down period. Slides were rinsed in distilled water and PBS. The samples were then blocked using Protein Block (Spring Bioscience) for 30 min. The sections were incubated with primary antibodies diluted in 2% BSA in PBS overnight in a humid chamber at 4°C. The slides were washed using the IF buffer (containing 0.05% Tween-20 and 0.2% Triton X-100 in PBS) and incubated with secondary antibodies diluted in 2% BSA in PBS for 1 h at room temperature. Following additional wash steps with the IF buffer, the slides were mounted with ProLong™ Diamond Antifade Mountant with DAPI (Invitrogen) to counterstain cell nuclei. Fluorescent images were acquired using ZEISS LSM 700 laser scanning confocal microscope with a 63X objective.

4.6 | Quantification of mRNA expression by quantitative real-time PCR

For selected parenchymal tissue samples, WM and GM fragments were separated by visual inspection and individually processed. Total RNA was extracted from derived cells and used for qPCR analysis as described in Healy et al., 2016 (Healy et al., 2016).

4.7 | Fluorescent-activated cell sorting

After the tissue from the white and gray matter was processed and the single-cell suspension was obtained, the cells were transferred into 96 well plates for FACS staining. Cells were first incubated with LIVE/DEAD fixable Aqua Dead Cell stain (Invitrogen, Cat# L34957) for 30 min at 4°C. After washing and blocking with mouse IgG (60 ug/ml, Thermofisher, Cat# 10400C) for 10 min at 4°C, cells were incubated with A2B5-APC(Miltenyi, Cat #130–093-582), O4-PE (Miltenyi, Cat# 130–117-823), HLA-DR-AF700 (BD Biosciences, Cat#561016), HLA-ABC-PacificBlue (Biolegend, Cat#311418), CD11b-PeCy7(eBiosciences, Cat#25–0118-42) for 20 min at 4°C. Appropriate isotype controls were used to assess non-specific fluorescence signals. The samples were acquired on the BD LSRFortessa Cell Analyzer FACS machine (BD Biosciences) and analyzed using FlowJo Software (FlowJo, https://www.flowjo.com/solutions/flowjo).

AUTHORS' CONTRIBUTION

M.Y. and J.P.A. contributed to the conception and design of the study, acquisition and analysis of data, figure preparation, and drafting of text. H.D and C.L. performed the FACS experiment. J.A.S. reviewed parenchymal samples used in this study. E.A. and MY developed the website. L.M.H., J.A.S., and T.E.K. contributed to study design and drafting of text. J.L., C.L.C., S.B., K.P., J.A.H., M.S., R.D., L.H., J.O., M.G., and C.S. contributed to the acquisition and analysis of data.

FUNDING INFORMATION

The study was supported by a grant (BRAVE in MS) from the International Progressive Multiple Sclerosis Alliance (J.P.A.)

CONFLICT OF INTEREST

The authors declare that they have no competing interests.

DATA AVAILABILITY STATEMENT

All data needed to evaluate the conclusions in the paper are present in the paper. The raw data of this study is available under the following accession numbers: Parenchymal brain samples (GSE160813), spinal cord samples (GSE162807). The data of SVZ samples will be available through direct contact with corresponding author after paper is being accepted. To facilitate the use of our scRNA-seq datasets, we have also developed a straightforward online tool for evaluating gene expression at single-cell resolution (https://stratton-lab.github.io/dataviz).

ORCID

Moein Yaqubi https://orcid.org/0000-0001-7299-5930
Julia Xiao Xuan Luo https://orcid.org/0000-0003-2838-1231
Qiao-Ling Cui https://orcid.org/0000-0002-2074-9655
Miltiadis Georgiopoulos https://orcid.org/0000-0001-8656-1412
Luke M. Healy https://orcid.org/0000-0001-9496-2216
Timothy E. Kennedy https://orcid.org/0000-0003-4454-5080

REFERENCES

Aprato, J., Sock, E., Weider, M., Elsesser, O., Fröb, F., & Wegner, M. (2020). Myrf guides target gene selection of transcription factor Sox10 during oligodendroglial development. *Nucleic Acids Research*, *48*, 1254–1270.

Arnett, H. A., Fancy, S. P. J., Alberta, J. A., Zhao, C., Plant, S. R., Kaing, S., Raine, C. S., Rowitch, D. H., Franklin, R. J. M., & Stiles, C. D. (2004). bHLH transcription factor Olig1 is required to repair demyelinated lesions in the CNS. *Science*, *306*(80), 2111–2115.

Bernstein, H.-G., Keilhoff, G., Dobrowolny, H., Guest, P. C., & Steiner, J. (2019). Perineuronal oligodendrocytes in health and disease: The journey so far. *Rev Neurosci*, *31*, 89–99. https://doi.org/10.1515/revneuro-2019-0020

Blighe K, Rana SLM. 2022. Enhanced volcano: Publication-ready volcano plots with enhanced colouring and labeling. *Github* [Internet]. Available from: https://github.com/kevinblighe/EnhancedVolcano

Cai, J., Zhu, Q., Zheng, K., Li, H., Qi, Y., Cao, Q., & Qiu, M. (2010). Co-localization of Nkx6.2 and Nkx2.2 homeodomain proteins in differentiated myelinating oligodendrocytes. *Glia*, *58*, 458–468.

Chen R, Wu X, Jiang L, Zhang Y. 2017. Single-cell RNA-Seq reveals hypothalamic cell diversity. *Cell Rep 18*:3227–3241. Available from: https://pubmed.ncbi.nlm.nih.gov/28355573

Couturier, C. P., Ayyadhury, S., Le, P. U., Nadaf, J., Monlong, J., Riva, G., Allache, R., Baig, S., Yan, X., Bourgey, M., Lee, C., Wang, Y. C. D., Wee Yong, V., Guiot, M.-C., Najafabadi, H., Misic, B., Antel, J., Bourque, G., Ragoussis, J., & Petrecca, K. (2020). Single-cell RNA-seq reveals that glioblastoma recapitulates a normal neurodevelopmental hierarchy. *Nat Commun*, *11*, 3406. https://doi.org/10.1038/s41467-020-17186-5

Darmanis S, Sloan SA, Zhang Y, Enge M, Caneda C, Shuer LM, Hayden Gephart MG, Barres BA, Quake SR. 2015. A survey of human brain transcriptome diversity at the single cell level. *Proc Natl Acad Sci 112*: 7285–7290. Available from: http://www.pnas.org/content/112/23/7285.abstract

Duncan ID, Radcliff AB, Heidari M, Kidd G, August BK, Wierenga LA. 2018. The adult oligodendrocyte can participate in remyelination. *Proc Natl Acad Sci 115*:E11807–E11816. Available from: http://www.pnas.org/content/115/50/E11807.abstract

Falcão, A. M., van Bruggen, D., Marques, S., Meijer, M., Jäkel, S., Agirre, E., Samudyata, F. E. M., Vanichkina, D. P., Ffrench-Constant, C., Williams, A., Guerreiro-Cacais, A. O., & Castelo-Branco, G. (2018). Disease-specific oligodendrocyte lineage cells arise in multiple sclerosis. *Nat Med*, *24*, 1837–1844. https://doi.org/10.1038/s41591-018-0236-y

de Faria, O., Dhaunchak, A. S., Kamen, Y., Roth, A. D., Kuhlmann, T., Colman, D. R., & Kennedy, T. E. (2019). TMEM10 promotes oligodendrocyte differentiation and is expressed by oligodendrocytes in human Remyelinating multiple sclerosis plaques. *Sci Rep*, *9*, 3606. https://doi.org/10.1038/s41598-019-40342-x

Fernandes, M. G. F., Luo, J. X. X., Cui, Q.-L., Perlman, K., Pernin, F., Yaqubi, M., Hall, J. A., Dudley, R., Srour, M., Couturier, C. P., Petrecca, K., Larochelle, C., Healy, L. M., Stratton, J. A., Kennedy, T. E., & Antel, J. P. (2021). Age-related injury responses of human oligodendrocytes to metabolic insults: Link to BCL-2 and autophagy pathways. *Commun Biol [Internet]*, *4*, 20. https://doi.org/10.1038/s42003-020-01557-1

Foerster, S., Hill, M. F. E., & Franklin, R. J. M. (2019). Diversity in the oligodendrocyte lineage: Plasticity or heterogeneity? *Glia*, *67*, 1797–1805. https://doi.org/10.1002/glia.23607

Franklin, R. J. M., & Ffrench-Constant, C. (2008). Remyelination in the CNS: From biology to therapy. *Nat Rev Neurosci*, *9*, 839–855. https://doi.org/10.1038/nrn2480

Fu M, McAlear TS, Nguyen H, Oses-Prieto JA, Valenzuela A, Shi RD, Perrino JJ, Huang T-T, Burlingame AL, Bechstedt S, Barres BA. 2019. The Golgi outpost protein TPPP nucleates microtubules and is critical for myelination. *Cell 179*:132-146.e14. Available from: https://doi.org/10.1016/j.cell.2019.08.025

Fulton, D. L., Denarier, E., Friedman, H. C., Wasserman, W. W., & Peterson, A. C. (2011). Towards resolving the transcription factor network controlling myelin gene expression. *Nucleic Acids Res*, *39*, 7974–7991. https://doi.org/10.1093/nar/gkr326

Habib, N., Avraham-Davidi, I., Basu, A., Burks, T., Shekhar, K., Hofree, M., Choudhury, S. R., Aguet, F., Gelfand, E., Ardlie, K., Weitz, D. A., Rozenblatt-Rosen, O., Zhang, F., & Regev, A. (2017). Massively parallel single-nucleus RNA-seq with DroNc-seq. *Nat Methods*, *14*, 955–958. https://doi.org/10.1038/nmeth.4407

Healy LM, Perron G, Won S-Y, Michell-Robinson MA, Rezk A, Ludwin SK, Moore CS, Hall JA, Bar-Or A, Antel JP. 2016. MerTK is a functional regulator of myelin phagocytosis by human myeloid cells. *J Immunol 196*:3375–3384. Available from: http://www.jimmunol.org/content/196/8/3375.abstract

Ishii A, Dutta R, Wark GM, Hwang S-I, Han DK, Trapp BD, Pfeiffer SE, Bansal R. 2009. Human myelin proteome and comparative analysis with mouse myelin. *Proc Natl Acad Sci 106*:14605–14610. Available from: http://www.pnas.org/content/106/34/14605.abstract

Jäkel, S., Agirre, E., Mendanha Falcão, A., van Bruggen, D., Lee, K. W., Knuesel, I., Malhotra, D., Ffrench-Constant, C., Williams, A., & Castelo-Branco, G. (2019). Altered human oligodendrocyte heterogeneity in multiple sclerosis. *Nature*, *566*, 543–547. https://doi.org/10.1038/s41586-019-0903-2

Kirby, L., Jin, J., Cardona, J. G., Smith, M. D., Martin, K. A., Wang, J., Strasburger, H., Herbst, L., Alexis, M., Karnell, J., Davidson, T., Dutta, R., Goverman, J., Bergles, D., & Calabresi, P. A. (2019). Oligodendrocyte precursor cells present antigen and are cytotoxic targets in inflammatory demyelination. *Nat Commun*, *10*, 3887. https://doi.org/10.1038/s41467-019-11638-3

Küspert, M., Hammer, A., Bösl, M. R., & Wegner, M. (2011). Olig2 regulates Sox10 expression in oligodendrocyte precursors through an evolutionary conserved distal enhancer. *Nucleic Acids Research*, *39*, 1280–1293.

Lake, B. B., Chen, S., Sos, B. C., Fan, J., Kaeser, G. E., Yung, Y. C., Duong, T. E., Gao, D., Chun, J., Kharchenko, P. V., & Zhang, K. (2018). Integrative single-cell analysis of transcriptional and epigenetic states in the human adult brain. *Nat Biotechnol*, *36*, 70–80. https://doi.org/10.1038/nbt.4038

Leong, S. Y., Rao, V. T. S., Bin, J. M., Gris, P., Sangaralingam, M., Kennedy, T. E., & Antel, J. P. (2014). Heterogeneity of oligodendrocyte

progenitor cells in adult human brain. *Ann Clin Transl Neurol*, *1*, 272–283. https://doi.org/10.1002/acn3.55

Luo, J. X. X., Cui, Q.-L., Yaqubi, M., Hall, J. A., Dudley, R., Srour, M., Addour, N., Jamann, H., Larochelle, C., Blain, M., Healy, L. M., Stratton, J. A., Sonnen, J. A., Kennedy, T. E., & Antel, J. P. (2022). Human oligodendrocyte myelination potential; relation to age and differentiation. *Ann Neurol*, *91*, 178–191. https://doi.org/10.1002/ana.26288

Marques S, van Bruggen D, Vanichkina DP, Floriddia EM, Munguba H, Väremo L, Giacomello S, Falcão AM, Meijer M, Björklund ÅK, Hjerling-Leffler J, Taft RJ, Castelo-Branco G. 2018. Transcriptional convergence of oligodendrocyte lineage progenitors during development. *Dev Cell 46*:504-517.e7. Available from: https://linkinghub.elsevier.com/retrieve/pii/S1534580718305586

Marques, S., Zeisel, A., Codeluppi, S., van Bruggen, D., Mendanha Falcão, A., Xiao, L., Li, H., Haring, M., Hochgerner, H., Romanov, R. A., Gyllborg, D., Munoz-Manchado, A. B., La Manno, G., Lonnerberg, P., Floriddia, E. M., Rezayee, F., Ernfors, P., Arenas, E., Hjerling-Leffler, J., … Castelo-Branco, G. (2016). Oligodendrocyte heterogeneity in the mouse juvenile and adult central nervous system. *Science*, *352*, 1326–1329. https://doi.org/10.1126/science.aaf6463

Martínez-Cerdeño, V., & Noctor, S. C. (2018). Neural progenitor cell terminology. *Front Neuroanat*, *12*, 1–8. https://doi.org/10.3389/fnana.2018.00104/full

Moon, K. R., van Dijk, D., Wang, Z., Gigante, S., Burkhardt, D. B., Chen, W. S., Yim, K., van den Elzen, A., Hirn, M. J., Coifman, R. R., Ivanova, N. B., Wolf, G., & Krishnaswamy, S. (2019). Visualizing structure and transitions in high-dimensional biological data. *Nat Biotechnol*, *37*, 1482–1492. https://doi.org/10.1038/s41587-019-0336-3

Pérez-Cerdá, F., Sánchez-Gómez, M. V., & Matute, C. (2015). Pío del Río Hortega and the discovery of the oligodendrocytes. *Front Neuroanat*, *9*, 92. https://doi.org/10.3389/fnana.2015.00092

Perlman, K., Couturier, C. P., Yaqubi, M., Tanti, A., Cui, Q.-L., Pernin, F., Stratton, J. A., Ragoussis, J., Healy, L., Petrecca, K., Dudley, R., Srour, M., Hall, J. A., Kennedy, T. E., Mechawar, N., & Antel, J. P. (2020). Developmental trajectory of oligodendrocyte progenitor cells in the human brain revealed by single cell RNA sequencing. *Glia*, *68*, 1291–1303.

Seeker LA, Bestard-Cuche N, Jäkel S, Kazakou N-L, Bøstrand SMK, Kilpatrick AM, Van Bruggen D, Kabbe M, Pohl FB, Moslehi Z, Henderson NC, Vallejos CA, La Manno G, Castelo-Branco G, Williams A. 2022. Marked regional glial heterogeneity in the human white matter of the central nervous system. bioRxiv [Internet]. Available from: https://doi.org/10.1101/2022.03.22.485367v1.abstract

Spaethling JM, Na Y-J, Lee J, Ulyanova A V, Baltuch GH, Bell TJ, Brem S, Chen HI, Dueck H, Fisher SA, Garcia MP, Khaladkar M, Kung DK, Lucas TH, O'Rourke DM, Stefanik D, Wang J, Wolf JA, Bartfai T, Grady MS, Sul J-Y, Kim J, Eberwine JH. 2017. Primary cell culture of Live Neurosurgically resected aged adult human brain cells and single cell Transcriptomics. *Cell Rep 18*:791–803. Available from: https://pubmed.ncbi.nlm.nih.gov/28099855

Stuart, T., Butler, A., Hoffman, P., Hafemeister, C., Papalexi, E., Mauck, W. M., Hao, Y., Stoeckius, M., Smibert, P., & Satija, R. (2019). Comprehensive integration of single-cell data. *Cell*, *177*, 1888–1902.e21. https://doi.org/10.1016/j.cell.2019.05.031

Szuchet, S., Nielsen, J. A., Lovas, G., Domowicz, M. S., de Velasco, J. M., Maric, D., & Hudson, L. D. (2011). The genetic signature of perineuronal oligodendrocytes reveals their unique phenotype. *Eur J Neurosci*, *34*, 1906–1922. https://doi.org/10.1111/j.1460-9568.2011.07922.x

Windrem, M. S., Nunes, M. C., Rashbaum, W. K., Schwartz, T. H., Goodman, R. A., McKhann, G., Roy, N. S., & Goldman, S. A. (2004). Fetal and adult human oligodendrocyte progenitor cell isolates myelinate the congenitally dysmyelinated brain. *Nat Med*, *10*, 93–97. https://doi.org/10.1038/nm974

Wu, T., Hu, E., Xu, S., Chen, M., Guo, P., Dai, Z., Feng, T., Zhou, L., Tang, W., Zhan, L., Fu, X., Liu, S., Bo, X., & Yu, G. (2021). clusterProfiler 4.0: A universal enrichment tool for interpreting omics data. *Innov [Internet]*, *2*, 100141. https://pubmed.ncbi.nlm.nih.gov/34557778

Yeung MSY, Djelloul M, Steiner E, Bernard S, Salehpour M, Possnert G, Brundin L, Frisén J. 2019. Dynamics of oligodendrocyte generation in multiple sclerosis. *Nature 566*:538–542. Available from: http://www.nature.com/articles/s41586-018-0842-3

Yu, G., Wang, L.-G., Han, Y., & He, Q.-Y. (2012). clusterProfiler: An R package for comparing biological themes among gene clusters. *Omi A J Integr Biol*, *16*, 284–287. https://doi.org/10.1089/omi.2011.0118

Yu Y, Chen Y, Kim B, Wang H, Zhao C, He X, Liu L, Liu W, Wu LMN, Mao M, Chan JR, Wu J, Lu QR. 2013. Olig2 targets chromatin remodelers to enhancers to initiate oligodendrocyte differentiation. *Cell [Internet] 152*:248–261. Available from: https://pubmed.ncbi.nlm.nih.gov/23332759

Zappia, L., & Oshlack, A. (2018). Clustering trees: A visualization for evaluating clusterings at multiple resolutions. *Gigascience*, *7*. https://doi.org/10.1093/gigascience/giy083

Zeisel A, Munoz-Manchado AB, Codeluppi S, Lonnerberg P, La Manno G, Jureus A, Marques S, Munguba H, He L, Betsholtz C, Rolny C, Castelo-Branco G, Hjerling-Leffler J, Linnarsson S. 2015. Cell types in the mouse cortex and hippocampus revealed by single-cell RNA-seq. *Science 347*:1138–1142. Available from: http://science.sciencemag.org/content/347/6226/1138.abstract

Zhao C, Ma D, Zawadzka M, Fancy SPJ, Elis-Williams L, Bouvier G, Stockley JH, de Castro GM, Wang B, Jacobs S, Casaccia P, Franklin RJM. 2015. Sox2 sustains recruitment of oligodendrocyte progenitor cells following CNS demyelination and primes them for differentiation during Remyelination. *J Neurosci 35*:11482–11499. Available from: http://www.jneurosci.org/content/35/33/11482.abstract

Zonouzi M, Berger D, Jokhi V, Kedaigle A, Lichtman J, Arlotta P. 2019. Individual oligodendrocytes show bias for inhibitory axons in the neocortex. *Cell Rep 27*:2799-2808.e3. Available from: https://www.sciencedirect.com/science/article/pii/S2211124719306291

SUPPORTING INFORMATION

Additional supporting information can be found online in the Supporting Information section at the end of this article.

How to cite this article: Yaqubi, M., Luo, J. X. X., Baig, S., Cui, Q.-L., Petrecca, K., Desu, H., Larochelle, C., Afanasiev, E., Hall, J. A., Dudley, R., Srour, M., Haglund, L., Ouellet, J., Georgiopoulos, M., Santaguida, C., Sonnen, J. A., Healy, L. M., Stratton, J. A., Kennedy, T. E., & Antel, J. P. (2022). Regional and age-related diversity of human mature oligodendrocytes. *Glia*, 1–12. https://doi.org/10.1002/glia.24230